

Author-prepared preprint version. The official article is available at:

Niklas Bauer, David Harings, Damian Mendroch, Jan Matrisch, Uwe Oberheide, Alexander Heisterkamp, “Extending the measurement range in ophthalmic linear optical coherence tomography using dual reference path interferometry”, Proceedings Volume 13300, Ophthalmic Technologies XXXV; 133000I(2025); <https://doi.org/10.1117/12.3046633>

Extending the Measurement Range in Ophthalmic Linear Optical Coherence Tomography using Dual Reference Path Interferometry

Niklas Bauer^a, David Harings^a, Damian Mendroch^a, Jan Matrisch^a, Uwe Oberheide^a,
and Alexander Heisterkamp^b

^aTechnische Hochschule Köln, Betzdorferstraße 2, 50679 Cologne, Germany

^bLeibniz Universität Hannover, Welfengarten 1, 30167 Hannover, Germany

Abstract

A fiber-based linear optical coherence tomography (LOCT) system employing a cost-effective CMOS camera has previously demonstrated high-resolution imaging suitable for retinal screening, including glaucoma monitoring. However, the system’s imaging depth was constrained to approximately 400 μm , insufficient for depth imaging of the optic nerve head (ONH), due to limitations imposed by the camera’s sensor size and pixel pitch. To overcome this limitation without replacing the economical and available sensor, we present a modification to the reference arm. By optimizing the utilization of the camera sensor’s vertical dimension, the system achieves an extended imaging depth, enabling the visualization of deeper tissue structures. Validation using an artificial eye model confirms that the modified LOCT system significantly enhances imaging depth while maintaining B-Scan quality. This advancement offers a cost-effective approach to extend the measurement range of LOCT systems, broadening their applicability in retinal imaging without altering the actual imaging sensor.

Keywords: OCT, LOCT, Retinal Imaging, Low-cost OCT

1 INTRODUCTION

In recent years, optical coherence tomography (OCT) systems have become an invaluable tool in the management of retinal diseases, such as glaucoma and age-related macular degeneration (AMD). The high resolution and depth sensitivity of OCT have greatly enhanced the ability to detect structural changes in the retina and underlying tissues at an early stage. This makes OCT an efficient tool for diagnosis. Beyond its diagnostic applications, OCT is used to track disease progression and guide therapeutic interventions[1]. However, the high cost of commercial OCT systems limits their accessibility, particularly for widespread use in regular monitoring outside of clinical settings. To address this limitation, efforts have been made to develop cost-effective alternatives. A promising low-cost alternative is the linear OCT (LOCT)[2]. In a previous study, a LOCT prototype was developed for glaucoma monitoring applications[3]. Despite its cost-effectiveness, the LOCT prototype lacks sufficient measurement depth to effectively monitor glaucoma progression. For sufficient depth imaging of the optic nerve head (ONH) and successful tracking of glaucoma, a measurement range exceeding 700 μm —and ideally approaching 1 mm, as seen in commercial OCT systems—is required[4][5]. With the LOCT’s current measurement range of 400 μm , a significant improvement is necessary to meet established standards. Since the measurement range in LOCT is highly dependent on sensor specifications and high-performance sensors with small pixels and a large number of pixels are rare and costly, it is necessary to develop quasi sensor-independent strategies to enhance the LOCT’s depth range. In this work, a new approach based on dual reference path interferometry is presented, which addresses these challenges and offers a pathway to achieving the desired measurement range in a cost-effective manner.

2 FUNDAMENTALS OF LOCT

The imaging depth in OCT is a critical parameter for depth-resolved imaging, as well as for diagnostic and monitoring applications. While the physical and technical factors influencing measurement depth in both Fourier-domain and Time-domain OCT systems are well-documented, these factors are less well known in LOCT, as it is not a commonly used technology [3][6]. As shown in Fig. 1, in LOCT, the depth-resolved information is obtained by tilting the reference wave by an angle α , thereby creating a variation in the optical path lengths ΔS along the illuminated width d on the sensor.

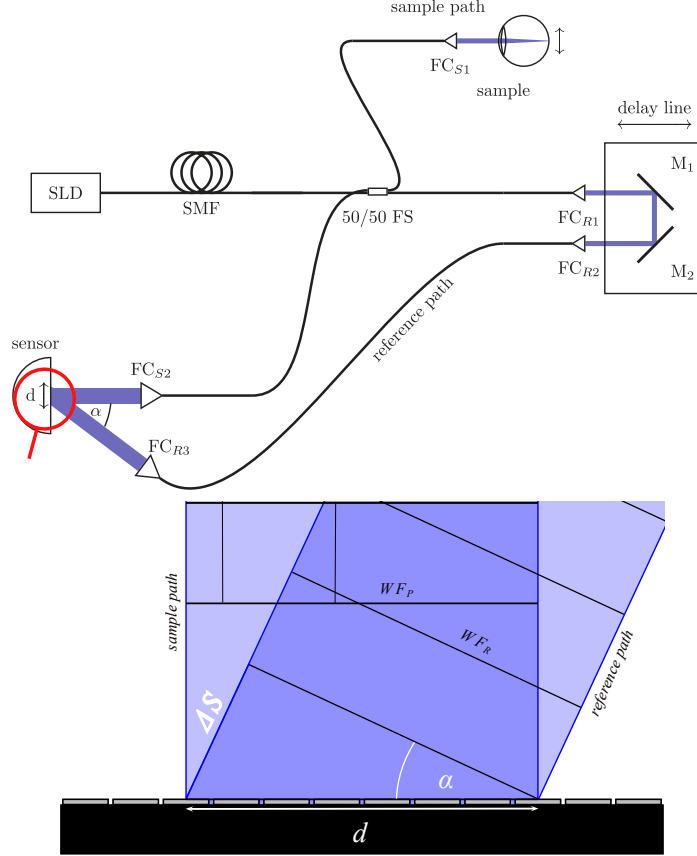


Figure 1: Top: Schematic set-up of LOCT prototype: SLD: Superluminescent Diode, SMF: Single Mode Fiber, FS: Fiber Splitter, FC: Fiber Collimator.

Bottom: Schematic representation of the superposition of the reference and sample waves on the sensor to illustrate the measurement range.

This results in an interference pattern given by Eq.(1).

$$I(\Delta S(\alpha, d)) = I_S + I_R + 2\sqrt{I_S I_R} \cos(k_0 \Delta S(\alpha, d)) \gamma(\Delta S(\alpha, d)) \quad (1)$$

By expressing the geometrical path difference ΔS through the tilting angle α and the illuminated width d , the interference pattern is given by Eq.(2).

$$I(\alpha, d) = I_S + I_R + 2\sqrt{I_S I_R} \cos(k_0 d \sin(\alpha)) \gamma(d, \sin(\alpha)) \quad (2)$$

The relevant depth information is encoded in the coherence function $\gamma(\Delta S(\alpha, d))$, or equivalently in the envelope of the interference pattern. The maximum imaging depth in the sample medium Δz_s is the one-way optical path difference. Since ΔS represents the geometric path difference and accounts for the fact that the light wave passes through the sample twice, the imaging depth must be scaled by a factor of 2 and by the refractive index of the sample n_s [2]. Consequently, the maximum imaging depth Δz_s is expressed as:

$$\Delta z_s = \frac{\Delta S}{2n_s} = \frac{d \sin(\alpha)}{2n_s} \quad (3)$$

As shown in Fig. 1, the illuminated width d can be described through sensor parameters such as the number of pixels N_{pix} in the illuminated width and the size of the pixels x_{pix} . Accordingly, Eq.(3) can be expressed as:

$$\Delta z_s = \frac{N_{pix} x_{pix} \sin(\alpha)}{2n_s} \quad (4)$$

In LOCT, resolving the modulation of the interference pattern g is essential for accurate depth imaging. To satisfy Nyquist's theorem, the interference pattern must be sampled by at least two pixels [7]. As a result, the maximum allowable pixel pitch, $\Delta x_{pixel_{max}}$, is given by:

$$\Delta x_{pixel_{max}} = \frac{g}{2} = \frac{\lambda_{min}}{2 \sin(\alpha)} \quad (5)$$

3 SUMMARY OF LOCT PROTOTYPE

Based on the theoretical background mentioned in Sec. 2, a low-cost LOCT system for ophthalmic applications was developed, as presented in a previous work [3]. For convenience, the main specifications are briefly summarized below.

- Sensor specs: $N_{pix} = 3682$, $x_{pix} = 2.4 \mu\text{m}$
- Angle between waves: $\alpha = 7.2^\circ$
- Mean refractive index of human ocular medium[8]: $n_s = 1.365$
- Resulting (measured) maximum imaging depth: $\Delta z_s = 405.7 \mu\text{m}$

While this system successfully enables depth imaging, as shown in Fig. 2, the achieved imaging depth remains significantly below the required $700 \mu\text{m}$ for glaucoma monitoring [4]. In theory, as described by Eq.(4), the imaging depth could be improved by either employing a sensor with a higher number of pixels N_{pix} or by increasing the angle α between the interfering waves. However, since the modulation of the interference pattern is inversely proportional to $\sin(\alpha)$, as shown by Eq.(5), an increase in α would necessitate a corresponding reduction in pixel size. Consequently, both approaches would require replacing the sensor, as sensors with a high pixel count and small pixel sizes are both costly and commercially limited in availability. Thus, a quasi sensor-independent solution was developed.

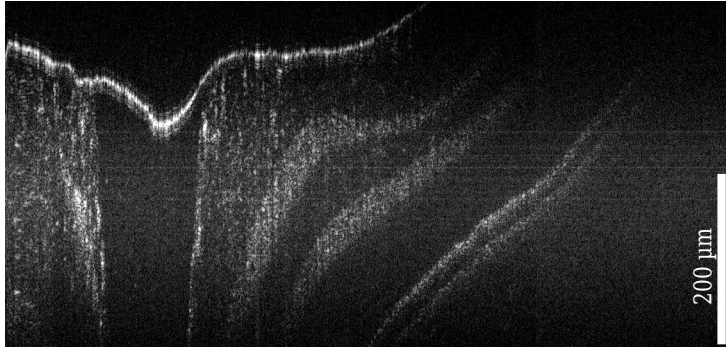


Figure 2: B-Scan of optic nerve head of an artificial OCT eye with LOCT prototype, $\Delta z_s = 405.7 \mu\text{m}$ [9]

4 MEASUREMENT RANGE ENHANCEMENT

The fundamental approach to extending the measurement range involves utilizing the otherwise unused vertical dimension of the camera sensor. Along the vertical axis, the data is largely redundant, requiring only a few pixels for post-processing and B-Scan calculation [3][10]. In contrast, the critical depth information is encoded along the horizontal axis of the sensor. To exploit the unused vertical dimension, the sensor area is divided into two distinct measurement areas. This modification is accomplished by converting the interferometer in the LOCT system into a dual reference path configuration, by introducing a second reference path through the addition of a delay line, as illustrated in Fig. 3. To prevent interference between the different reference waves, they are spatially separated along the vertical axis of the sensor by focusing them through cylindrical lenses (CL_1 and CL_2) on the sensor and by having polarizations perpendicular to each other (delay line 1: vertical linear polarization, delay line 2: horizontal linear polarization). The bottom part of Fig. 3 shows the interference pattern generated by a mirror as a sample. As observed, there are two distinct interference patterns. Since the optical paths are nearly identical, the interference patterns appear at nearly the same depth. To extend the overall measurement range, an additional optical path delay, corresponding to the maximum measurement range Δz_s , must be introduced between delay line 1 and delay line 2.

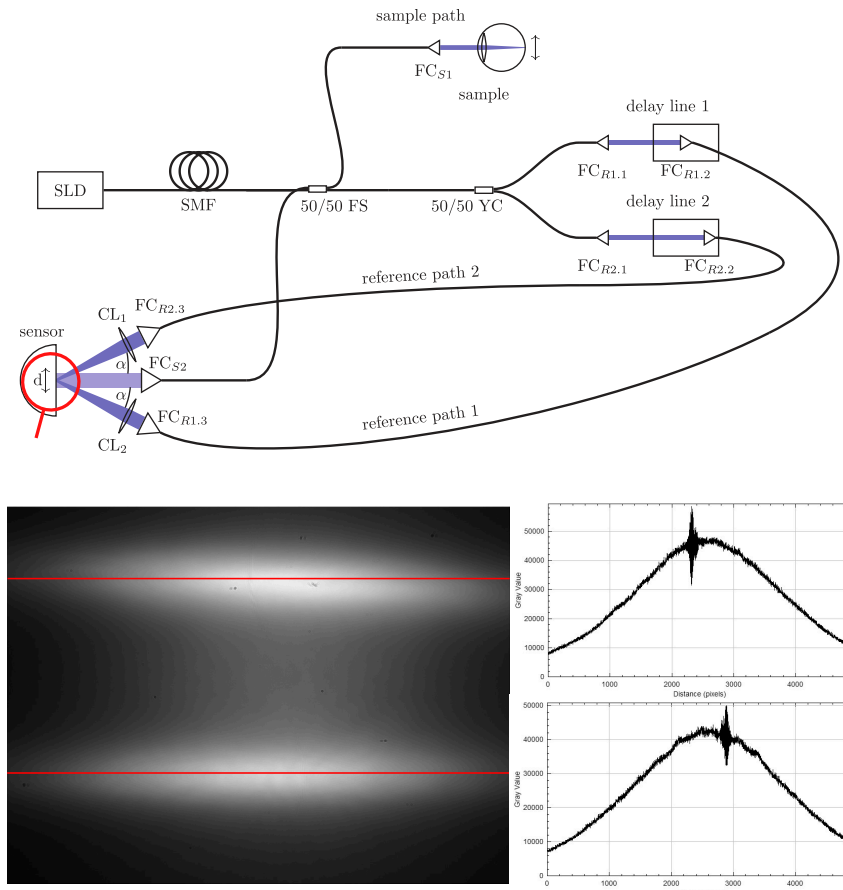


Figure 3: Top: Dual Reference Path LOCT for extended measurement range. SLD: Superluminescent Diode, SMF: Single Mode Fiber, FS: Fiber Splitter, YC: Y-Coupler, FC: Fiber Collimator, CL: Cylindric lens.

Bottom: Sensor image of measurement enhanced LOCT system with interference pattern. Plots show intensity cross-section of red lines.

This results in two different interference pattern for delay line 1 (I_{SDL1}) and delay line 2 (I_{SDL2}) given by Eq.(6) and Eq.(7)

$$I_{SDL1} = I_S + I_{RDL1} + 2\sqrt{I_S I_{RDL1}} \cos(k_0 d \sin(\alpha)) \gamma(\Delta s(\alpha, d)) \quad (6)$$

$$I_{SDL2} = I_S + I_{RDL2} + 2\sqrt{I_S I_{RDL2}} \cos(k_0(d \sin(\alpha) + \Delta z_s)) \gamma(\Delta s(\alpha, d, \Delta z_s)) \quad (7)$$

Therefore resulting in two measurement ranges ($MR1$ and $MR2$) at different depths.

$$\begin{aligned} 0 &\leq MR1 \leq \Delta z_s \\ \Delta z_s &\leq MR2 \leq 2\Delta z_s \end{aligned}$$

5 RESULTS

To test the extension of the measurement range and verify its functionality, B-Scans of an artificial eye were taken. Figure 4 presents a comparison between the B-Scans of an artificial OCT eye obtained using the unenhanced system (left) and the enhanced system (right). Both B-Scans capture approximately the same region of the optic nerve head (ONH). Minor differences may occur due to the current lack of precise OCT beam tracking via a funduscopy system.

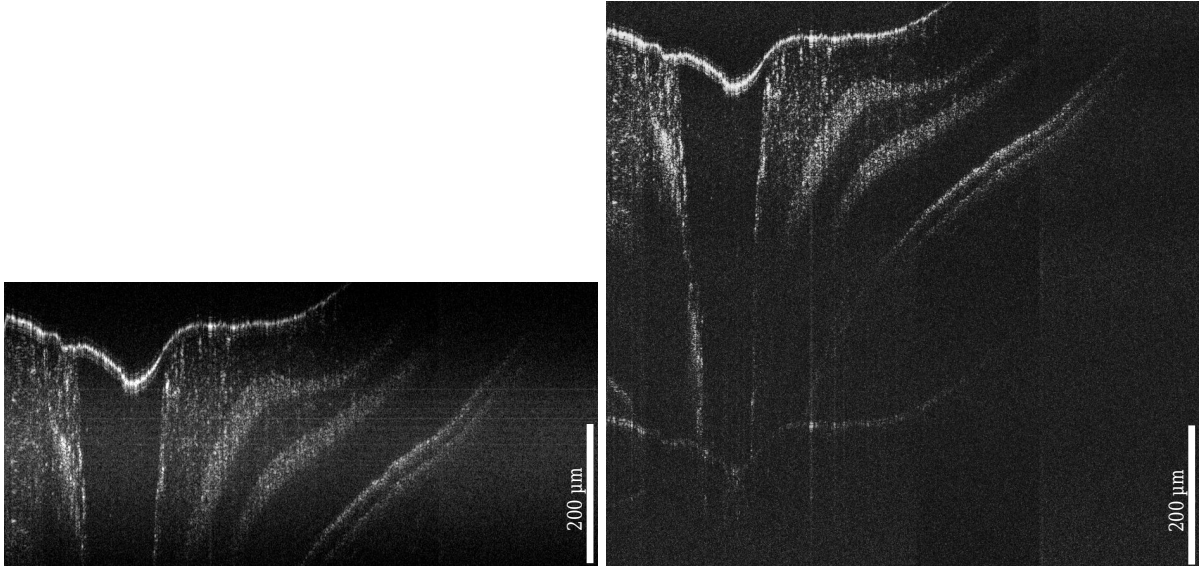


Figure 4: Comparison between B-Scan of unenhanced prototype (right) and enhanced prototype (left)

The measurement range of the enhanced LOCT system has been doubled, as depicted in Fig. 4. In Fig. 5, a second B-Scan was acquired, demonstrating a measured range of $\Delta z = 811.4 \mu\text{m}$ with an enclosed angle $\alpha = 7.2^\circ$ and a total amount of illuminated pixels of $2N_{pix} = 7364$, resulting in an illuminated width of $d = 17.7 \mu\text{m}$. This provides a measurement ranges of $0 \mu\text{m} \leq MR1 \leq 405.7 \mu\text{m}$ and $405.7 \mu\text{m} \leq MR2 \leq 811.4 \mu\text{m}$ for a total measurement range of $\Delta z_s = 811.4 \mu\text{m}$. Regarding the quality of the B-Scans, a slight sensitivity loss can be observed in deeper tissue layers due to reduced light propagation, which is a common characteristic of depth imaging. Additionally, as the updated system operates with two separate measurement areas, it is crucial to carefully match the intensity in both reference paths to the intensity of the sample path. This ensures consistent contrast and B-Scan quality across the entire measurement area.

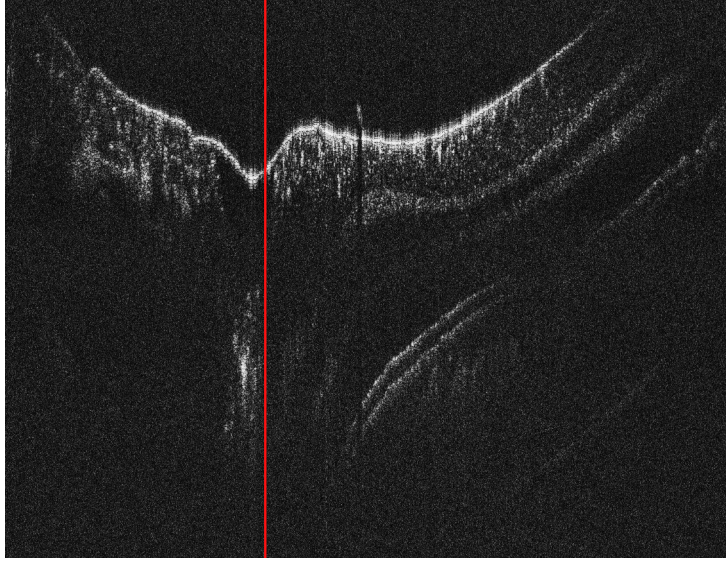


Figure 5: B-Scan of optic nerve head of an artificial OCT eye with enhanced measurement range LOCT prototype, length of red line marks $811.4\ \mu\text{m}$

6 CONCLUSION

This work successfully enhanced the imaging depth of the LOCT system through the implementation of dual-reference path interferometry. By doubling the measurement range to approximately $800\ \mu\text{m}$, the system now meets the requirements for glaucoma monitoring. However, the introduction of dual-reference path interferometry increased system complexity, necessitating careful balancing of intensities between the reference and sample paths. This step is critical to maintaining high contrast and ensuring consistent B-Scan quality across the entire measurement area, thereby minimizing image degradation. Despite its complexity, the system retains a low-cost design by employing a quasi sensor-independent approach and off-the-shelf components. While the current system serves as a proof of concept and does not yet match the performance of commercial Fourier-domain OCT systems, it demonstrates significant potential for further improvements in imaging depth. For instance, a multi-reference path interferometry setup could achieve an x -fold increase in imaging range, offering promising opportunities for advanced future applications. Additionally, the system allows for non-adjacent measurement depths within the sample, which could enable simultaneous imaging of different regions of the human eye. Future work will focus on adapting the system for in vivo imaging of the human eye and integrating LOCT with a funduscopy system [11][12]. These developments will build on the current achievements and bring the system closer to clinical applications.

ACKNOWLEDGMENTS

This research received funding from the German Federal Ministry of Education and Research (German: Bundesministerium für Bildung und Forschung - BMBF), under funding reference number 13FH141KX1.

References

- [1] Z. M. Dong, G. Wollstein, and J. S. Schuman, “Clinical utility of optical coherence tomography in glaucoma,” *Investigative Ophthalmology & Visual Science*, vol. 57, no. 9, p. OCT 556, 2016.
- [2] P. Koch, G. Hüttmann, H. Schleiermacher, J. Eichholz, and E. Koch, “Linear optical coherence tomography system with a downconverted fringe pattern,” *Optics Letters*, vol. 29, p. 1644, 2004.
- [3] N. Bauer, D. Mendroch, D. Harings, J. Matrisch, U. Oberheide, and A. Heisterkamp, “Development of a linear optical coherence tomography low-cost system for ophthalmic applications,” *SPIE Biomedical Spectroscopy, Microscopy, and Imaging III*, pp. 13006–84, 2024.

- [4] J. A. Vilensky, W. Robertson, and C. A. Suarez-Quian, *The Clinical Anatomy of the Cranial Nerves: The Nerves of On Old Olympus Towering Top*. Ames, Iowa, USA.: Wiley-Blackwell, 2015 (1st Edition).
- [5] W. Drexler and J. G. Fujimoto, “Introduction to optical coherence tomography,” in *Optical Coherence Tomography* (W. Drexler and J. G. Fujimoto, eds.), pp. 1–40, Berlin, Germany: Springer, 2008.
- [6] J. Izatt and M. Choma, “Theory of optical coherence tomography,” in *Optical Coherence Tomography* (W. Drexler and J. G. Fujimoto, eds.), pp. 47–72, Berlin, Germany: Springer, 2008.
- [7] J. W. Goodman, *Introduction to Fourier Optics*. Greenwood Village, United States: Roberts & Company Publishers, 2005 (3rd Edition).
- [8] J. Bille and W. Schlengel, “Medizinische Laserphysik,” in *Medizinische Physik* (J. Bille and W. Schlengel, eds.), Berlin, Germany: Springer, 2005.
- [9] D. E. Lankenau, “Model eye for Optical Coherence Tomography.” Modell-Augen-Manufaktur, 2024 <https://modell-augen-manufaktur.de>. (Accessed: 13.03.2024).
- [10] D. Mendroch, N. Bauer, D. Harings, and A. Heisterkamp, “Deconvolution-based image enhancement for optical coherence tomography,” *SPIE Biomedical Spectroscopy, Microscopy, and Imaging III*, pp. 13006–83, 2024.
- [11] D. Harings, N. Bauer, D. Mendroch, U. Oberheide, and H. Lubatschowski, “Precise control of eye movement for real-time video funduscopy and OCT using dynamic fixation patterns,” *SPIE BiOS Ophthalmic Technologies XXXV*, pp. 13300–59, 2025.
- [12] D. Mendroch, N. Bauer, D. Harings, and A. Heisterkamp, “Robust real-time retinal tracking for ophthalmic applications,” *SPIE BiOS Ophthalmic Technologies XXXV*, pp. 13300–74, 2025.